



Published in final edited form as:

Nat Genet. 2016 June ; 48(6): 648–656. doi:10.1038/ng.3558.

The ciliopathy-associated CPLANE proteins direct basal body recruitment of intraflagellar transport machinery

Michinori Toriyama¹, Chanjae Lee¹, S. Paige Taylor², Ivan Duran², Daniel H. Cohn³, Ange-Line Bruel⁴, Jacqueline M. Tabler¹, Kevin Drew¹, Marcus R. Kelley⁵, Sukyoung Kim¹, Tae Joo Park^{1,**}, Daniella Braun⁶, Ghislaine Pierquin⁷, Armand Biver⁸, Kerstin Wagner⁹, Anne Malfroot¹⁰, Inusha Panigrahi¹¹, Brunella Franco^{12,13}, Hadeel Adel Al-lami¹⁴, Yvonne Yeung¹⁴, Yeon Ja Choi¹⁵, University of Washington Center for Mendelian Genomics¹⁶, Yannis Duffourd⁴, Laurence Faivre^{4,17}, Jean-Baptiste Rivière^{4,18}, Jiang Chen¹⁵, Karen J. Liu¹⁴, Edward M. Marcotte¹, Friedhelm Hildebrandt⁶, Christel Thauvin-Robinet^{4,18}, Deborah Krakow³, Peter K. Jackson⁵, and John B. Wallingford^{1,*}

¹ Dept. of Molecular Biosciences, University of Texas at Austin

² Departments of Orthopaedic Surgery, Human Genetics and Obstetrics and Gynecology, David Geffen School of Medicine at UCLA, Los Angeles, California, USA

³ Department of Molecular Cell and Developmental Biology, University of California at Los Angeles, California, USA, 90095

⁴ EA4271GAD Genetics of Developmental Anomalies, FHU-TRANSLAD, Medecine Faculty, Burgundy University, F-21079 Dijon, France

⁵ Stanford University School of Medicine, Baxter Laboratory, Department of Microbiology & Immunology, Stanford, California 94305

⁶ HHMI and Department of Medicine, Boston Children's Hospital, Harvard Medical School, Boston, MA 02115, USA

⁷ Clinical genetics centre, University Hospital Center, Liège, Belgian

Users may view, print, copy, and download text and data-mine the content in such documents, for the purposes of academic research, subject always to the full Conditions of use:http://www.nature.com/authors/editorial_policies/license.html#terms

* Corresponding author: Patterson Labs, University of Texas, 2401 Speedway, Austin, Tx. 78712, Wallingford@austin.utexas.edu, 512-232-2784.

** Current Address: UNIST, Ulsan, Korea

Author Contributions:

Michinori Toriyama contributed to design, execution and interpretation of the overall research plan, with special emphasis on all frog embryo experiments and in vitro binding assays. He also contributed to writing the manuscript. Chanjae Lee designed, performed and interpreted live-imaging of IFT particles in axonemes and contributed to other imaging experiments in *Xenopus*. Kevin Drew and Edward M. Marcotte provided protein structural models. Jacqueline M. Tabler, Jiang Chen and Karen J. Liu contributed to design execution and interpretation of mouse genetic data. Marcus R. Kelley contributed to the execution and analysis of the proteomic data. Tae Joo Park contributed to *Xenopus* studies. S. Paige Taylor, Ivan Duran, Daniel H. Cohn, Ange-Line Bruel, Daniella Braun, Ghislaine Pierquin, Armand Biver, Kerstin Wagner, Anne Malfroot, Inusha Panigrahi, Brunella Franco, Hadeel Adel Al-lami, Yvonne Yeung, Yeon Ja Choi, University of Washington Center for Mendelian Genomics, Yannis Duffourd, Laurence Faivre, Jean-Baptiste Rivière contributed to collection of human patient and sequencing data. Friedhelm Hildebrandt, Christel Thauvin-Robinet, and Deborah Krakow contributed to design, execution and interpretation of human genetic data. Peter K. Jackson contributed to coordinating the overall research effort with a focus on design and interpretation of the proteomic screen and contributed to writing the manuscript. John Wallingford coordinated the overall research effort, oversaw experimental design and interpretation, and wrote the manuscript.

- ⁸ Pediatric unit, Hospital Center, Luxemburg
- ⁹ Cardiological Pediatric unit, Hospital Center, Luxemburg
- ¹⁰ Clinic of Pediatric Respiratory Diseases, Infectious Diseases, Travel Clinic and Cystic Fibrosis Clinic at the Universitair Ziekenhuis UZ Brussel, Belgium
- ¹¹ Department of Pediatrics Advanced, Pediatric Centre Pigmer, Chandigarh, India
- ¹² Department of Medical Translational Sciences, Division of Pediatrics, Federico II University of Naples, Italy
- ¹³ Telethon Institute of Genetics and Medicine-TIGEM, Naples Italy
- ¹⁴ Dept. of Craniofacial and Stem Cell Biology, Dental Institute, King's College London
- ¹⁵ Departments of Pathology and Dermatology, Stony Brook University, Stony Brook, NY 11794
- ¹⁶ University of Washington Center for Mendelian Genomics; Full list of members available at: <http://www.mendelian.org/mendelian-center/university-of-washington>
- ¹⁷ Clinical genetics centre and Eastern referral centre for developmental anomalies and malformative syndromes, FHU-TRANSLAD, Children Hospital, CHU Dijon, F-21079 Dijon, France
- ¹⁸ Laboratory of Molecular Genetics, FHU-TRANSLAD, PTB, CHU Dijon, F-21079 Dijon, France

Summary

Cilia use microtubule-based intraflagellar transport (IFT) to organize intercellular signaling. The ciliopathies are a spectrum of human disease resulting from defects in cilia structure or function. Mechanisms regulating assembly of ciliary multiprotein complexes and their transport to the base of cilia remain largely unknown. Combine proteomics, *in vivo* imaging, and genetic analysis of proteins linked to planar cell polarity (Inturned, Fuzzy, WDPCP), we identified and characterized a new genetic module, which we term CPLANE (ciliogenesis and planar polarity effector) and an extensive associated protein network. CPLANE proteins physically and functionally interact with the poorly understood ciliopathy protein Jbts17 at basal bodies, where they act to recruit a specific subset of IFT-A proteins. In the absence of CPLANE, defective IFT-A particles enter the axoneme, and IFT-B trafficking is severely perturbed. Accordingly, mutation of CPLANE genes elicits specific ciliopathy phenotypes in mouse models and is associated with novel ciliopathies in human patients.

Introduction

The ciliopathies are a broad class of human diseases that share an etiology of defective cilia structure or function. These diseases span skeletal anomalies, craniofacial defects, cystic kidneys, blindness, obesity, and other presentations, highlighting the wide array of physiological functions that require components of the cilium^{1,2}.

Like all organelles, cilia are assembled and maintained by multi-protein machines. For example, the BBSome is a large complex involved in trafficking of ciliary membrane proteins³; the Nphp and Mks/B9 complexes assemble the ciliary transition zone, which

controls access to the cilium^{4,5}; and dynein arms drive motile ciliary beating⁶. Likewise, the intraflagellar transport (IFT) system, which links cargos to microtubule motors for transport into and out of cilia, is comprised of two multi-protein complexes, IFT-A and IFT-B⁷⁻¹¹, IFT-A and IFT-B are frequently described as controlling retrograde and anterograde traffic, respectively. However, both anterograde kinesin motors and retrograde dynein motors can physically associate with IFT-A^{7,12-14}, and recent studies highlight the role of IFT-A in ciliary entry and anterograde traffic^{15,16}. IFT-A and IFT-B are each composed of a multi-protein “core” in addition to more loosely-bound “peripheral” components^{15,17-19}.

While recent papers have begun to define the interactions between IFT complexes and their cargoes (e.g. Ref. ^{20,21}), substantial questions remain concerning the mechanisms by which IFT proteins are recruited to the base of cilia and assembled into IFT trains. Indeed, ciliopathies can result from defects in cytosolic factors that facilitate dynein arm or BB transport and assembly²²⁻²⁸, yet little is known about similar factors that may act on IFT. For example, basal bodies in *Ttbk2* mutant mice fail to recruit certain subunits of the IFT-A and IFT-B complexes, but they also fail to remove CP110, a key initial step for ciliogenesis²⁹. Likewise, *Odf1*, *Cep83/Ccdc41*, and *C2cd3* are implicated in recruiting certain IFT-B subunits to the basal body, but the specificity of these proteins for IFT recruitment is hard to discern, as only a small subset of IFT proteins has been examined in these mutants and these proteins have pleiotropic roles in ciliogenesis³⁰⁻³².

Here, we combine proteomics, *in vivo* cell biology, mouse models and human genetics to characterize a novel mechanism governing basal body recruitment and assembly of IFT-A. This novel regulatory module is formed by specific protein-protein interactions among *Intu*, *Fuz*, and *Wdpcp*, well-conserved proteins that control planar cell polarity (PCP) in *Drosophila* and govern ciliogenesis in vertebrates³³⁻³⁷ (Fig. 1A). We term this new module the “CPLANE,” for ciliogenesis and planar polarity effectors. We show that this module also includes the poorly understood ciliopathy protein *Jbts17*, which we show recruits CPLANE to basal bodies where it acts specifically by recruiting the IFT-A peripheral proteins. In the absence of CPLANE function, the IFT-A core denuded of peripheral components still undergoes normal bi-directional transport, though the movement of IFT-B is severely impaired. Finally, examination of mutant mice and ciliopathy alleles from human patients reinforce the connection between CPLANE proteins, *Jbts17*, and the IFT-A machinery, demonstrating that CPLANE plays a broad and essential role in ciliogenesis and human ciliopathies.

Results

Intu, *Fuz*, and *Wdpcp* are deeply conserved and are essential for vertebrate ciliogenesis (Fig. 1a)^{36,37}. To gain unbiased insights into their molecular functions, LAP-tagged versions of each were stably expressed in ciliated mouse kidney IMCD3 cells, lysates were prepared, and interacting proteins were affinity purified (Supplementary Fig. 1a,b). In addition, similar experiments were performed using diverse IFT-A and ciliopathy related proteins as baits. Mass-spectroscopy revealed the enrichment of the bait protein for each pull-down (Supplementary Fig. 1c, d; Supp. Dataset 1), and none of the baits were copurified with over 30 unrelated control proteins, although all baits did bring down common contaminants

(Supplementary Fig. 1e). From this experiment, we identified a set of roughly 250 proteins that were individually pulled down by each of the three CPLANE proteins (Supplementary Fig. 2a).

The CPLANE interactome

We identified an extensive interaction network for the CPLANE proteins that involved a wide array of protein machines, including dynein subunits, clathrin adaptors, and chaperonins, among others (Fig. 1b and Supplementary Fig. 2b-d). Given that CPLANE proteins are essential for vertebrate ciliogenesis^{36,37}, we were surprised to find only selective links to known ciliogenesis proteins. No links were found within the combined CPLANE interactome to many major ciliary machines, including the IFT-B complex, the BBSome, the inversin compartment, and transition zone B9 complex. An exception was the intraflagellar transport complex A (IFT-A), as between them, pulldown for Intu, Fuz and Wdpcp identified all six subunits of the IFT-A complex (Fig. 1b, c and Supplementary Fig. 2c), though no IFT-B proteins were found. Moreover, while pulldown of IFT-A proteins themselves also efficiently returned other IFT-A proteins, pulldowns with six other ciliogenesis-related baits did not (Supp. Fig. 1d). These data suggest that CPLANE may regulate IFT-A function, which we address below.

Most strongly enriched in all CPLANE pulldowns were the CPLANE proteins themselves, with Intu, Fuz, and Wdpcp reciprocally co-purified in all combinations (Supp Figs. 1c and 2d; Supp. Table 1). By contrast, these three proteins were entirely absent from pull-downs of six additional ciliopathy related proteins (Supp. Fig. 1c). Interaction among some CPLANE proteins has also been observed in high-throughput screens of human proteins^{38,39}. Moreover, the interactions are conserved in *Drosophila*⁴⁰, though these proteins have no apparent role in ciliogenesis in that animal. In addition, the Rsg1 GTPase, which we had previously observed as a Fuz interacting protein^{38,39,41}, was also strongly associated with Intu and Wdpcp (Supp. Fig. 1c).

Finally, among the most strongly enriched proteins in the CPLANE interactomes was the largely uncharacterized ciliopathy protein Jbts17 (also called C5orf42)(Fig. 1b and Supplementary Figs. 1c and 2c). This novel protein is associated with Joubert, Oral-Facial-Digital (OFD), and Meckel Gruber syndromes⁴²⁻⁴⁵, and one recent paper identifies it as a component of the transition zone⁴⁶. We confirmed interaction between Jbts17 and all three CPLANE proteins by co-IP of *in vitro* translated proteins (Supp. Fig. 2e). Because so little is known of Jbts17, we explored its link to the CPLANE proteins in more detail.

CPLANE protein localization at the base of cilia

Jbts17 is evolutionarily conserved (Fig. 1a) and implicated in varying ciliopathies, but its function remains largely undefined. In *Xenopus*, *Jbts17* was expressed in ciliated tissues (not shown), and knockdown using anti-sense morpholino-oligonucleotides (MOs) to disrupt splicing resulted in ciliopathy-related developmental defects, including failure of neural tube closure, defective Hedgehog signaling, and defective left/right patterning (Fig. 2a-c and Supplementary Fig. 3a,b). Accordingly, ciliogenesis was disrupted in the developing neural tube, in the node, and in multiciliated cells (MCCs)(Fig. 2d-f). CRISPR-based disruption of

Jbts17 also disrupted ciliogenesis, and co-injection of mRNA encoding GFP-Jbts17 rescued both the neural tube defects and ciliogenesis defects resulting from MO-based knockdown (Fig. 2f and Supplementary Fig. 3a, h).

Given the physical association of Fuz, Intu, and Wdpcp with Jbts17 and Rsg1 (Supp. Fig. 1c), we explored the interrelationships among these proteins in *Xenopus* MCCs, which provide an effective platform for *in vivo* ciliary cell biology. Intu, Fuz, Rsg1, and Jbts17 localized robustly around basal bodies but were difficult to detect in axonemes (Fig. 2g). Super-resolution imaging revealed that GFP-Jbts17 was present in a ring surrounding the basal body, as marked by centrin4-BFP; this ring was similar to that formed by the distal appendage marker Cep164 (Fig. 2h). However, Jbts17 knockdown did not significantly affect recruitment of the distal appendage proteins Cep164 or Ofd1, the transition zone marker Mks1, or the basal body docking protein Hook2 (Supplementary Fig. 3g).

To assess the functional relationships of these proteins, we knocked each CPLANE protein down using MOs previously validated by mouse knockouts (see Methods) and then examined basal body localization of the remaining CPLANE members. Our data place Rsg1 at the bottom of the hierarchy: Its localization was lost from basal bodies after knockdown of any CPLANE protein, yet its own knockdown did not affect basal body recruitment of any other component (Fig. 2j and Supplementary Fig. 3c-f). Wdpcp and Intu held clear positions upstream of Fuz and Rsg1, but downstream of Jbts17. Interestingly, Wdpcp and Intu were also each required for the other's basal body localization. The role of Fuz was more complicated; unlike the other CPLANE proteins Fuz did not require Jbts17 for localization to basal bodies, and while loss of Fuz did disrupt basal body localization of Intu and Rsg1, it did not affect Wdpcp. These data provide an initial framework for the hierarchy of CPLANE protein functions.

A Jbts17 disease allele disrupts Intu localization

Jbts17 is mutated in ciliopathies, so we asked if a disease-causing allele of Jbts17 would disrupt CPLANE function by examining a *Xenopus* cognate of a human Joubert syndrome-associated truncation of Jbts17. The R1569* truncation (equivalent to R1602 in humans⁴⁵; Supp. Fig. 4a) failed to localize to basal bodies, though another disease associated truncation R2406* localized normally, allowing us to map the basal body localization domain of Jbts17 to amino acids 1770-2318 (Supp. Fig. 4b). The pathogenicity of the R1569* truncation was apparent, because while expression of full-length Jbts17 efficiently rescues NTDs resulting from Jbts17 knockdown, expression of Jbts17-R1569* did not (Supplementary Fig. 3a). Linking this embryological defect to cell biological function, Jbts17-R1569* also failed to localize to basal bodies (Supplementary Fig. 4b) and unlike wild type, expression of Jbts17-R1569* could not rescue basal body recruitment of Intu after Jbts17 knockdown (Supplementary Fig. 4c). Thus, the Jbts17 disease allele fails to support CPLANE localization and function.

CPLANE recruits peripheral IFT-A proteins to basal bodies

To understand the mechanisms by which CPLANE proteins impact ciliogenesis, we returned to our proteomic dataset. We were intrigued by associations between CPLANE proteins and

the IFT machinery (Fig. 1b), because while we previously implicated Fuz and Rsg1 in IFT^{47,48}, their mechanism of action remained ill-defined. CPLANE proteins did not interact with IFT-B components, but rather specifically interacted with both the IFT-A core and peripheral IFT-A subunits (Fig. 1b and Supplementary Fig. 1c). Nothing is known about the regulation of peripheral sub-unit interaction with the IFT-A core, but we reasoned that by interacting with both, CPLANE could facilitate IFT-A function. Because CPLANE localizes to basal bodies, we tested this notion by assessing basal body recruitment of all six IFT-A proteins after CPLANE disruption.

Strikingly, *Jbts17* knockdown specifically disrupted the recruitment of the peripheral IFT-A subunits to the basal body. The levels of *Ift139*, *Ift121* and *Ift43* at basal bodies were dramatically reduced after *Jbts17* knockdown, though recruitment of the three IFT-A core proteins *Ift140*, *Ift144*, *Ift122* was not disrupted (Fig. 3 and Supplementary Fig. 5a). In fact, recruitment of *Ift122* was consistently increased (Fig. 3b,c). Though IFT-B is also composed of core and peripheral components, *Jbts17* knockdown did not disrupt recruitment of either the peripheral IFT-B proteins *Ift20*, *Ift80*, and *Cluap1*, or the core IFT-B protein *Ift81* (Fig. 3c and Supplementary Fig. 5b). Finally, the link between *Jbts17* and IFT-A is likely relevant to disease pathology, because while full-length *Jbts17* expression rescued the loss of IFT-A basal body recruitment after *Jbts17* knockdown, the Joubert-associated *Jbts17-R1569** truncation did not (Supplementary Fig. 4d).

Defective IFT-B trafficking in the absence of CPLANE

IFT particles exchange rapidly between axonemes and a cytoplasmic pool around the basal body, so we were curious to know what effect failure to recruit peripheral IFT-A proteins to basal bodies after CPLANE loss would have on IFT trafficking in the axoneme. We used high-speed confocal imaging to assess IFT in MCCs and found that disruption of either *Jbts17* or *Wdpcp* disrupted IFT-B movement, as we previously found for *Fuz*⁴⁷. Kymography revealed that both peripheral and core components of IFT-B formed stationary accumulations (Fig. 4a, b; Supplementary Fig. 5f), and quantitative microscopy confirmed a significant enrichment of total IFT-B levels in the axoneme (Supp. Fig. 5h).

These accumulations are reminiscent of the effect of genetic disruption of IFT-A^{9,10}. However, the mechanisms by which peripheral IFT-A proteins impact the movement of the IFT-A core has not been examined in detail, and overall, very little is known about the dynamics of IFT-A in vertebrates. We therefore also examined the effect of CPLANE loss on the dynamics of IFT-A peripheral and core proteins in the axoneme. We found that peripheral IFT-A proteins that were not recruited to basal bodies were likewise absent from axonemes after *Jbts17* knockdown, consistent with a role for CPLANE in assembly of peripheral subunits onto the IFT-A core (Supplementary Fig. 5e). By contrast, IFT-A core proteins were not only present in axonemes at normal levels after *Jbts17* knockdown (Supp. Fig. 5d, 5h), but they also underwent bi-directional transport (Fig. 4c, d; Supp. Fig. 5g), suggesting that the core was intact and could associate with both anterograde and retrograde motors. Similar effects on IFT-A and IFT-B were observed after *Wdpcp* knockdown (Supplementary Fig. 5f,g). These data suggest that CPLANE acts by recruiting peripheral IFT-A proteins to the basal body for assembly onto the IFT-A core.

OFD Syndrome phenotypes in mouse CPLANE mutants

Together with our proteomic data from mammalian cultured cells, the *in vivo* imaging data from *Xenopus* suggest that *Intu*, *Fuz*, and *Wdpcp* are intimately associated with *Jbts17*, which is the major gene mutated in human Oral-Facial-Digital Syndrome Type 6 (OFD6)⁴³. Key diagnostic features of OFD6 include high arched palate, tongue hamartoma, and polydactyly characterized by Y-shaped metacarpals⁴⁹. Examining these same features in *Fuz* mutant mice, we consistently observed high arched palates, lobulated tongues and Y-shaped metacarpals (Fig. 5a-d;f, h)(see also ref. ⁵⁰). We also observed Y-shaped metacarpals and defects in tongue and palate morphology in *Wdpcp* mutants (Fig. 5e, g). These genetic data linking CPLANE components to developmental defects characteristic of OFD are consistent with our proteomic link between CPLANE and *Jbts17*.

Human CPLANE genes are mutated in diverse ciliopathies

Our data argue for a functional and physical association of CPLANE proteins with *Jbts17* on the one hand, and with retrograde IFT machinery on the other. We therefore examined CPLANE gene sequences in the exomes of human ciliopathy patients, focusing on OFD for its connection to *Jbts17* (Ref. ⁴³) and on Short-Rib Polydactyly Syndrome (SRPS) for its association to IFT-A (Refs. ^{51,52}).

OFD VI, for which *Jbts17* is the major gene⁴³, shares substantial phenotypic overlap with OFD II, including high arched palate, tongue hamartomas, and Y-shaped metacarpals^{53,54}. Consistent with our data above, exome sequencing of OFD patients with these characteristics revealed disease-associated mutations in both *WDPCP* and *INTU*. In one patient, a 5-year-old male presenting with facial dysmorphism, tongue hamartoma, high arched palate, tooth abnormalities, and postaxial polydactyly, we found trans-heterozygous mutations in *WDPCP*. One mutation was a frameshift (c.526_527delTT; Leu176Ilefs*21), and the other, a missense mutation (c.160G>A; p.Asp54Asn) predicted to alter splicing by Human Splice Finder and ASSP (Fig. 6a,b and Supplementary Table 2a). Sanger sequencing confirmed the variants and compound heterozygosity for *WDPCP* by parental segregation (Fig. 6a). The altered aspartic acid residue (D54) of *WDPCP* is highly conserved (Supplementary Fig. 6a) and has been associated with atypical OFD in one previous patient⁵⁵, but no disease associated alleles of *WDPCP* have yet been tested functionally. We therefore expressed these proteins in *Xenopus* MCCs and found that the frame-shift allele resulted in total loss of protein, while the point mutation led to a consistent but more modest defect in protein stability (Fig. 6c).

We also examined a 10-year-old male presenting with facial dysmorphisms, tongue nodular tags, high arched palate, and bilateral central Y-shaped metacarpals (Supplementary Fig. 6b and Supplementary Table 2a). Exome sequencing revealed a homozygous frameshift mutation (c.396delT; p.Asn132Lysfs*11) in the *INTU* gene, and Sanger sequencing confirmed that the homozygous *INTU* variant segregated with the phenotype (Supplementary Fig. 6c). Brain MRI for both OFD patients showed no cerebellar abnormality, but cardiac ultrasound revealed aortic coarctation and tetralogy of Fallot in OFD patients with CPLANE mutations (Supplementary Table 2a), consistent with recent data implicating CPLANE genes in cardiac malformation⁵⁶.

In addition, we identified a homozygous missense mutation (p.Ala452Thr) in *INTU* in a child with nephronophthisis and growth retardation. The boy, who presented with end-stage renal failure at 10 yrs. of age, was the only affected child of three in a consanguineous family (Supplementary Table 2a). The identified allele segregated with the affected status, and homozygosity mapping revealed that the genomic locus of *INTU* was located within a stretch of homozygosity on chromosome 4 (Supplementary Fig. 6d and data not shown). This change is in a relatively poorly conserved residue (Supplementary Fig. 6e), suggesting that it may be a hypomorphic allele. We also identified a heterozygous mutation (p.Glu365Gly) in *WDPCP* in a boy with cerebellar vermis hypoplasia, ataxia, and retinal dystrophy (Supplementary Table 2a), which may be a modifying allele contributing to this ciliopathy.

Finally, we examined exomes of individuals with SRPS and identified an affected patient with compound heterozygosity for two *INTU* mutations confirmed by Sanger sequencing (c. 1063G>T; p.Glu355* and c. 1499A>C; p.Glu500Ala) (Fig. 6d, e; Supp. Fig. 6f). The affected individual was born pre-term at 30-weeks with multiple congenital anomalies, including wide-open fontanel, microphthalmia, tongue hamartomas, and tetralogy of Fallot (Supplementary Table 2b). Radiographic analyses showed multiple skeletal anomalies, including short horizontal ribs, shortened long bones with smooth edges, and pre- and post axial polydactyly (Fig. 6e and Supplementary Table 2b). To confirm that the identified alleles caused the patient's disease, we examined the function of the *INTU* mutants. The Glu355* allele failed to localize to basal bodies when expressed in *Xenopus* MCCs (Fig. 6f), and while the Glu500A mutation did not affect basal body localization, it did significantly impair the ability of the protein to recruit Ift43 (Fig 6g, h).

Another case, presented with strikingly similar SRPS features (Supplementary Fig. 6g,h and Supplementary Table 1b) and a single truncating mutation in *INTU* was confirmed by Sanger sequencing (c. 826C>T; p.Gln276*). This change was inherited from the unaffected mother (Figure S6i), but despite extensive analysis, no other changes were found in *INTU*. We examined over 500 changes in the patient's genome that segregated with the phenotype, and we found only a single change in a gene previously associated with SRPS, a heterozygous change in *WDR35* (IFT121). This change (c.932G>T; p.Trp311Leu) was confirmed by Sanger sequencing and was inherited from the unaffected father (Supplementary Fig. 6i), and this residue is invariant in vertebrates (Supplementary Fig. 6j). The clinical presentation of this patient was remarkably similar to the individual with compound heterozygosity for *INTU* mutations (Supplementary Table 2b). The most striking similarity was the distinct polydactyly; while most SRPS patients have 6-7 fingers and toes, these two patients both had 9-10. Thus, while we cannot rule out a role for mutations in unknown ciliopathy genes, the known role for *WDR35* in SRPS, our finding of a role for *INTU* in SRPS, and our finding of physical and functional interactions between IFT-A and CPLANE lead us to suggest that SRPS in this patient results from digenic inheritance of mutations in *WDR35* and *INTU*.

Discussion

Here, we characterize an essential but poorly understood protein module, which we term CPLANE (Ciliogenesis and Planar Polarity Effector). The CPLANE proteins Intu, Fuz, and Wdpcp/Fritz are deeply conserved in animal evolution (Fig. 1a) and were first identified as PCP proteins in *Drosophila*^{33-37,40}. In vertebrates, mutation of these genes elicits ciliogenesis defects, and while their role in PCP remains murky, recent reports do suggest that Wdpcp and Intu may govern the localization of core PCP proteins⁵⁷⁻⁵⁹. Here, we combined proteomics in mammalian cell culture, *in vivo* cell biology in *Xenopus*, and genetic analysis in both mice and humans to demonstrate that the CPLANE is an important physical and functional unit governing a specific facet of ciliogenesis, namely the recruitment of IFT-A proteins to the base of cilia and the insertion of complete IFT-A particles into the axoneme (Fig. 7a,b).

Guided by our proteomic screen, imaging experiments here revealed that in the absence of CPLANE, peripheral IFT-A proteins fail to localize to basal bodies and do not assemble onto the IFT-A core. This connection between CPLANE and IFT-A is strengthened by genetic data linking CPLANE proteins to SRPS, which is generally associated with defects in IFT-A^{51,52}. CPLANE does not traffic along axonemes, arguing that it is not a component of the IFT particle itself, a result supported by the fact that CPLANE proteins associate relatively strongly with one another in our proteomic data, but comparatively weakly with IFT proteins (Supplementary Fig. 1c). Together, these data argue that CPLANE facilitates IFT-A recruitment and assembly at basal bodies, though the precise mechanisms by which it acts remain to be determined.

One possibility is that CPLANE may direct cytoplasmic transport of IFT-A proteins to the base of cilia. This idea is supported by the many links to cytoplasmic dynein machinery in our proteomics (Fig. 1; Supp. Fig. 2). A second line of evidence comes from computational modeling of protein structures (see Methods), which suggests that CPLANE proteins contain structural domains common in vesicle trafficking machinery (Supp. Fig. 7). Fuz contains a longin domain, and Intu is predicted to fold into a Sec23/24 domain. Likewise, Wdpcp is predicted to form an alpha solenoid attached to a beta-propeller, a configuration present in coat proteins, as well as IFT and BBSome subunits⁶⁰. Finally, Jbts17 is an enormous protein (3167 amino acids) and can be threaded onto multiple protein models, including a Sec23/24 fold, a beta-propeller fold, and an importin domain.

On the other hand, the CPLANE proteins may instead impact IFT-A at the level of protein stability and assembly. This possibility is supported by our proteomic data linking Intu, Fuz, and Wdpcp individually to all eight subunits of the CCT chaperone complex (Fig. 1b; Table 1). This latter mechanism would be particularly intriguing, because similar mechanisms have been proposed linking protein folding to assembly of dynein arms^{22,23} and the BBSome^{27,28}. Importantly, as is true for the CPLANE proteins, disruption of cytosolic assembly factors for dynein arms and the BBSome also cause ciliopathies. This latter possibility is especially exciting because, despite this long history of study, cytosolic factors facilitating basal body recruitment and assembly of IFT particles have not been described.

We also found that peripheral IFT-A proteins were not present in axonemes after CPLANE knockdown, though IFT-A core proteins entered axonemes and trafficked bi-directionally. Because we also observed accumulations of IFT-B in axonemes similar to that following direct disruption of IFT-A⁹⁻¹¹, our data argue that the peripheral components are essential for association of IFT-B with IFT-A, at least during retrograde transport (Figs. 7a,b). This role for the peripheral IFT-A proteins raises interesting questions concerning the mechanism of IFT-B anterograde transport, because biochemical data suggest that heterotrimeric kinesin also associates with IFT particles via the IFT-A^{7,13}. Given that IFT-B moves into axonemes and accumulates there after CPLANE knockdown (Supp. Fig. 5c), it may be that the role for peripheral proteins in linking IFT-A to IFT-B is specific to retrograde transport, consistent with the known remodeling of IFT particles upon turnaround^{11,12}. Alternatively, homodimeric kinesin 2 associates directly with IFT-B in *C. elegans*, and while the situation in vertebrates is less clear^{61,62}, IFT-B could move into cilia after CPLANE knockdown via direct association with the homodimeric Kif17. Finally, the role for diffusion in axonemal transport is only now coming into focus^{20,63}, so it is at least possible that IFT-B in these cases moves in the axoneme could move in such a manner.

Finally, our data implicate CPLANE in diverse ciliopathies. Because SRPS is generally associated with disruption of IFT-A^{51,52}, our identification of *INTU* mutations in SRPS patients provides a genetic complement to our proteomic and cell biological linkage of CPLANE to IFT-A. Our identification of CPLANE mutations in OFD patients similarly parallels the physical and functional association of CPLANE with Jbts17. Additional insights into the mechanism of CPLANE mutation in human disease will certainly emerge as we venture deeper into the CPLANE protein interaction network. For example, *Wdpcp* mutations have been found in at least one patient with Bardet- Biedl Syndrome³⁶, so the links between CPLANE proteins and CCT are interesting since BBS6, 10 and 12 also interact with CCT^{27,28}. Our data may also shed light on the still murky role of *FUZ* in human neural tube defects⁶⁴. Finally, our data suggest that the CPLANE may be relevant not only to congenital defects, but also to infectious disease, since recent data link *Fuz* and the endocytic machinery to alphavirus entry⁶⁵, and we observed extensive interactions between CPLANE and the vesicle trafficking machinery (Fig. 1b; Supp. Fig. 2b). In sum, our data establish the CPLANE as a novel ciliogenic protein module with significant roles in development and human disease.

Experimental procedures

Details of the experimental procedures can be found in the Supplementary Material online. Briefly, the methods used here were essentially those described previously. Immunoprecipitation of LAP-Tagged CPLANE proteins was performed as described in ref. ⁴. General methods for experiments with *Xenopus* were performed as described in ref ^{36,37}. Specifically, imaging of IFT proteins at basal bodies and time-lapse imaging of IFT were performed as per Ref. ⁴⁷. Exome sequencing was performed essentially as per Ref. ⁴ and Ref.⁴³.

Supplementary Material

Refer to Web version on PubMed Central for supplementary material.

Acknowledgements

We thank the patients and their families; the IntegraGen society for exome analysis; NHLBI GO Exome Sequencing Project which produced and provided exome variant calls for comparison: Lung GO Sequencing Project (HL-102923), WHI Sequencing Project (HL-102924), the Broad GO Sequencing Project (HL-102925), Seattle GO Sequencing Project (HL-102926) and Heart GO Sequencing Project (HL-103010). We thank Biological Resources Center – Ferdinand Cabanne (Dijon, France) for fibroblasts centralization and storage. Sequencing was provided by the University of Washington Center for Mendelian Genomics (UW CMG) and was funded by the NHGRI and NHLBI (Grant 1U54 HG006493) to Drs. Debbie Nickerson, Jay Shendure, and Michael Bamshad. This work was supported by grants from the following: Uehara Memorial Foundation Fellowship to M.T.; an NIDCR NRSA to J.M.T.; the French Rare Diseases Foundation, French Ministry of Health (PHRC national 2010-A01014-35 to C.T.-R), and Regional Council of Burgundy to C.T.-R.; NIDDK (DK1068306) to F.H., who is an HHMI Investigator, a Doris Duke Distinguished Clinical Scientist, and the Warren E. Grupe Professor; NIAMS (AR061485) to J.C. ; BBSRC (BB/K010492/1) and MRC (MR/L017237/1) to K.J.L.; NIH, NSF, CPRIT, and the Welch Foundation (F-1515) to E.M.M.; R01AR066124, March of Dimes and Joseph Drown Foundation, NIH/NCATS UCLA CTSA Grant UL1TR000124 to D.K.; R01AR062651 to D.H.C.; NIGMS (GM114276), Baxter Laboratory, and Stanford Department of Research to P.K.J.; NIGMS and NHLBI to J.B.W., who was an HHMI Early Career Scientist.

References

- Hildebrandt F, Benzing T, Katsanis N. Ciliopathies. *N Engl J Med*. 2011; 364:1533–43. [PubMed: 21506742]
- Oh EC, Katsanis N. Cilia in vertebrate development and disease. *Development*. 2012; 139:443–8. [PubMed: 22223675]
- Nachury MV, et al. A core complex of BBS proteins cooperates with the GTPase Rab8 to promote ciliary membrane biogenesis. *Cell*. 2007; 129:1201–13. [PubMed: 17574030]
- Sang L, et al. Mapping the NPHP-JBTS-MKS protein network reveals ciliopathy disease genes and pathways. *Cell*. 2011; 145:513–28. [PubMed: 21565611]
- Garcia-Gonzalo FR, et al. A transition zone complex regulates mammalian ciliogenesis and ciliary membrane composition. *Nat Genet*. 2011; 43:776–84. [PubMed: 21725307]
- Kobayashi D, Takeda H. Ciliary motility: the components and cytoplasmic preassembly mechanisms of the axonemal dyneins. *Differentiation*. 2012; 83:S23–9. [PubMed: 22154137]
- Cole DG, et al. Chlamydomonas kinesin-II-dependent intraflagellar transport (IFT): IFT particles contain proteins required for ciliary assembly in *Caenorhabditis elegans* sensory neurons. *J Cell Biol*. 1998; 141:993–1008. [PubMed: 9585417]
- Kozminski KG, Johnson KA, Forscher P, Rosenbaum JL. A motility in the eukaryotic flagellum unrelated to flagellar beating. *Proc Natl Acad Sci U S A*. 1993; 90:5519–23. [PubMed: 8516294]
- Pazour GJ, Wilkerson CG, Witman GB. A dynein light chain is essential for the retrograde particle movement of intraflagellar transport (IFT). *J Cell Biol*. 1998; 141:979–92. [PubMed: 9585416]
- Piperno G, et al. Distinct mutants of retrograde intraflagellar transport (IFT) share similar morphological and molecular defects. *J Cell Biol*. 1998; 143:1591–601. [PubMed: 9852153]
- Iomini C, Babaev-Khaimov V, Sassaroli M, Piperno G. Protein particles in *Chlamydomonas* flagella undergo a transport cycle consisting of four phases. *J Cell Biol*. 2001; 153:13–24. [PubMed: 11285270]
- Pedersen LB, Geimer S, Rosenbaum JL. Dissecting the molecular mechanisms of intraflagellar transport in *chlamydomonas*. *Curr Biol*. 2006; 16:450–9. [PubMed: 16527740]
- Rompolas P, Pedersen LB, Patel-King RS, King SM. *Chlamydomonas* FAP133 is a dynein intermediate chain associated with the retrograde intraflagellar transport motor. *J Cell Sci*. 2007; 120:3653–65. [PubMed: 17895364]
- Ou G, Blacque OE, Snow JJ, Leroux MR, Scholey JM. Functional coordination of intraflagellar transport motors. *Nature*. 2005; 436:583–7. [PubMed: 16049494]

15. Mukhopadhyay S, et al. TULP3 bridges the IFT-A complex and membrane phosphoinositides to promote trafficking of G protein-coupled receptors into primary cilia. *Genes Dev.* 2010; 24:2180–93. [PubMed: 20889716]
16. Liem KF Jr, et al. The IFT-A complex regulates Shh signaling through cilia structure and membrane protein trafficking. *J Cell Biol.* 2012; 197:789–800. [PubMed: 22689656]
17. Behal RH, et al. Subunit interactions and organization of the *Chlamydomonas reinhardtii* intraflagellar transport complex A proteins. *J Biol Chem.* 2012; 287:11689–703. [PubMed: 22170070]
18. Lucker BF, et al. Characterization of the intraflagellar transport complex B core: direct interaction of the IFT81 and IFT74/72 subunits. *J Biol Chem.* 2005; 280:27688–96. [PubMed: 15955805]
19. Taschner M, Bhogaraju S, Lorentzen E. Architecture and function of IFT complex proteins in ciliogenesis. *Differentiation.* 2012; 83:S12–22. [PubMed: 22118932]
20. Craft JM, Harris JA, Hyman S, Kner P, Lechtreck KF. Tubulin transport by IFT is upregulated during ciliary growth by a cilium-autonomous mechanism. *J Cell Biol.* 2015; 208:223–37. [PubMed: 25583998]
21. Bhogaraju S, et al. Molecular basis of tubulin transport within the cilium by IFT74 and IFT81. *Science.* 2013; 341:1009–12. [PubMed: 23990561]
22. Tarkar A, et al. DYX1C1 is required for axonemal dynein assembly and ciliary motility. *Nat Genet.* 2013; 45:995–1003. [PubMed: 23872636]
23. Omran H, et al. Ktu/PF13 is required for cytoplasmic pre-assembly of axonemal dyneins. *Nature.* 2008; 456:611–6. [PubMed: 19052621]
24. Mitchison HM, et al. Mutations in axonemal dynein assembly factor DNAAF3 cause primary ciliary dyskinesia. *Nat Genet.* 2012; 44:381–9. S1–2. [PubMed: 22387996]
25. Horani A, et al. Whole-exome capture and sequencing identifies HEATR2 mutation as a cause of primary ciliary dyskinesia. *Am J Hum Genet.* 2012; 91:685–93. [PubMed: 23040496]
26. Diggle CP, et al. HEATR2 plays a conserved role in assembly of the ciliary motile apparatus. *PLoS Genet.* 2014; 10:e1004577. [PubMed: 25232951]
27. Seo S, et al. BBS6, BBS10, and BBS12 form a complex with CCT/TRiC family chaperonins and mediate BBSome assembly. *Proc Natl Acad Sci U S A.* 2010
28. Zhang Q, Yu D, Seo S, Stone EM, Sheffield VC. Intrinsic protein-protein interaction-mediated and chaperonin-assisted sequential assembly of stable bardet-biedl syndrome protein complex, the BBSome. *J Biol Chem.* 2012; 287:20625–35. [PubMed: 22500027]
29. Goetz SC, Liem KF Jr, Anderson KV. The spinocerebellar ataxia-associated gene Tau tubulin kinase 2 controls the initiation of ciliogenesis. *Cell.* 2012; 151:847–58. [PubMed: 23141541]
30. Ye X, Zeng H, Ning G, Reiter JF, Liu A. C2cd3 is critical for centriolar distal appendage assembly and ciliary vesicle docking in mammals. *Proc Natl Acad Sci U S A.* 2014; 111:2164–9. [PubMed: 24469809]
31. Singla V, Romaguera-Ros M, Garcia-Verdugo JM, Reiter JF. Odf1, a human disease gene, regulates the length and distal structure of centrioles. *Dev Cell.* 2010; 18:410–24. [PubMed: 20230748]
32. Joo K, et al. CCDC41 is required for ciliary vesicle docking to the mother centriole. *Proc Natl Acad Sci U S A.* 2013; 110:5987–92. [PubMed: 23530209]
33. Adler PN, Charlton J, Park WJ. The *Drosophila* tissue polarity gene intumed functions prior to wing hair morphogenesis in the regulation of hair polarity and number. *Genetics.* 1994; 137:829–36. [PubMed: 8088527]
34. Collier S, Gubb D. *Drosophila* tissue polarity requires the cell-autonomous activity of the fuzzy gene, which encodes a novel transmembrane protein. *Development.* 1997; 124:4029–37. [PubMed: 9374400]
35. Collier S, Lee H, Burgess R, Adler P. The WD40 repeat protein fritz links cytoskeletal planar polarity to frizzled subcellular localization in the *Drosophila* epidermis. *Genetics.* 2005; 169:2035–45. [PubMed: 15654087]
36. Kim SK, et al. Planar Cell Polarity Acts Through Septins to Control Collective Cell Movement and Ciliogenesis. *Science.* 2010; 329:1337–1340. [PubMed: 20671153]

37. Park TJ, Haigo SL, Wallingford JB. Ciliogenesis defects in embryos lacking inturned or fuzzy function are associated with failure of planar cell polarity and Hedgehog signaling. *Nat Genet.* 2006; 38:303–11. [PubMed: 16493421]
38. Huttlin EL, et al. The BioPlex Network: A Systematic Exploration of the Human Interactome. *Cell.* 2015; 162:425–40. [PubMed: 26186194]
39. Rual JF, et al. Towards a proteome-scale map of the human protein-protein interaction network. *Nature.* 2005; 437:1173–8. [PubMed: 16189514]
40. Wang Y, Yan J, Lee H, Lu Q, Adler PN. The proteins encoded by the *Drosophila* Planar Polarity Effector genes inturned, fuzzy and fritz interact physically and can re-pattern the accumulation of “upstream” Planar Cell Polarity proteins. *Dev Biol.* 2014
41. Gray RS, et al. The planar cell polarity effector Fuz is essential for targeted membrane trafficking, ciliogenesis and mouse embryonic development. *Nat Cell Biol.* 2009; 11:1225–32. [PubMed: 19767740]
42. Alazami AM, et al. Molecular characterization of Joubert syndrome in Saudi Arabia. *Hum Mutat.* 2012; 33:1423–8. [PubMed: 22693042]
43. Lopez E, et al. C5orf42 is the major gene responsible for OFD syndrome type VI. *Hum Genet.* 2014; 133:367–77. [PubMed: 24178751]
44. Shaheen R, et al. Genomic analysis of Meckel-Gruber syndrome in Arabs reveals marked genetic heterogeneity and novel candidate genes. *Eur J Hum Genet.* 2013; 21:762–8. [PubMed: 23169490]
45. Srour M, et al. Mutations in C5ORF42 cause Joubert syndrome in the French Canadian population. *Am J Hum Genet.* 2012; 90:693–700. [PubMed: 22425360]
46. Damerla RR, et al. Novel *Jbts17* mutant mouse model of Joubert syndrome with cilia transition zone defects and cerebellar and other ciliopathy related anomalies. *Hum Mol Genet.* 2015
47. Brooks E, Wallingford JB. Control of vertebrate intraflagellar transport by the planar cell polarity effector Fuz. *J. Cell Biol.* 2012; 198:37–45. [PubMed: 22778277]
48. Brooks ER, Wallingford JB. The Small GTPase Rsg1 is important for the cytoplasmic localization and axonemal dynamics of intraflagellar transport proteins. *Cilia.* 2013; 2:13. [PubMed: 24192041]
49. Gurrieri F, Franco B, Toriello H, Neri G. Oral-facial-digital syndromes: review and diagnostic guidelines. *Am J Med Genet A.* 2007; 143A:3314–23. [PubMed: 17963220]
50. Tabler JM, et al. Fuz mutant mice reveal shared mechanisms between ciliopathies and FGF-related syndromes. *Dev Cell.* 2013; 25:623–35. [PubMed: 23806618]
51. Merrill AE, et al. Ciliary abnormalities due to defects in the retrograde transport protein DYNC2H1 in short-rib polydactyly syndrome. *Am J Hum Genet.* 2009; 84:542–9. [PubMed: 19361615]
52. Mill P, et al. Human and mouse mutations in WDR35 cause short-rib polydactyly syndromes due to abnormal ciliogenesis. *Am J Hum Genet.* 2011; 88:508–15. [PubMed: 21473986]
53. Hsieh YC, Hou JW. Oral-facial-digital syndrome with Y-shaped fourth metacarpals and endocardial cushion defect. *Am J Med Genet.* 1999; 86:278–81. [PubMed: 10482880]
54. Panigrahi I, Das RR, Kulkarni KP, Marwaha RK. Overlapping phenotypes in OFD type II and OFD type VI: report of two cases. *Clin Dysmorphol.* 2013; 22:109–14. [PubMed: 23459408]
55. Saari J, Lovell MA, Yu HC, Bellus GA. Compound heterozygosity for a frame shift mutation and a likely pathogenic sequence variant in the planar cell polarity-ciliogenesis gene WPCP in a girl with polysyndactyly, coarctation of the aorta, and tongue hamartomas. *Am J Med Genet A.* 2014
56. Li Y, et al. Global genetic analysis in mice unveils central role for cilia in congenital heart disease. *Nature.* 2015
57. Cui C, Chatterjee B, Lozito T, Zhang Z, Lo CW. Wdpcp, a PCP Protein Required for Ciliogenesis, Regulates Directional Cell Migration and Cell Polarity by Direct Modulation of the Actin Cytoskeleton. *PLoS Biol.* 2013; 11:e1001720. [PubMed: 24302887]
58. Butler MT, Wallingford JB. Control of vertebrate core planar cell polarity protein localization and dynamics by Prickle 2. *Development.* 2015; 142:3429–39. [PubMed: 26293301]
59. Zilber Y, et al. The PCP effector Fuzzy controls ciliary assembly and signaling by recruiting Rab8 and Dishevelled to the primary cilium. *Mol Biol Cell.* 2013; 24:555–65. [PubMed: 23303251]

60. van Dam TJ, et al. Evolution of modular intraflagellar transport from a coatomer-like progenitor. *Proc Natl Acad Sci U S A*. 2013; 110:6943–8. [PubMed: 23569277]
61. Pan X, et al. Mechanism of transport of IFT particles in *C. elegans* cilia by the concerted action of kinesin-II and OSM-3 motors. *J Cell Biol*. 2006; 174:1035–45. [PubMed: 17000880]
62. Snow JJ, et al. Two anterograde intraflagellar transport motors cooperate to build sensory cilia on *C. elegans* neurons. *Nat Cell Biol*. 2004; 6:1109–13. [PubMed: 15489852]
63. Harris JA, Liu Y, Yang P, Kner P, Lechtreck KF. Single particle imaging reveals IFT-independent transport and accumulation of EB1 in *Chlamydomonas* flagella. *Mol Biol Cell*. 2015
64. Seo JH, et al. Mutations in the planar cell polarity gene, Fuzzy, are associated with neural tube defects in humans. *Hum Mol Genet*. 2011
65. Ooi YS, Stiles KM, Liu CY, Taylor GM, Kielian M. Genome-wide RNAi screen identifies novel host proteins required for alphavirus entry. *PLoS Pathog*. 2013; 9:e1003835. [PubMed: 24367265]
66. Moody SA, Kline MJ. Segregation of fate during cleavage of frog (*Xenopus laevis*) blastomeres. *Anat Embryol (Berl)*. 1990; 182:347–62. [PubMed: 2252221]
67. Zeng H, Hoover AN, Liu A. PCP effector gene *Inturned* is an important regulator of cilia formation and embryonic development in mammals. *Dev Biol*. 2010; 339:418–28. [PubMed: 20067783]
68. Karpinka JB, et al. Xenbase, the *Xenopus* model organism database; new virtualized system, data types and genomes. *Nucleic Acids Res*. 2015; 43:D756–63. [PubMed: 25313157]
69. Park TJ, Mitchell BJ, Abitua PB, Kintner C, Wallingford JB. Dishevelled controls apical docking and planar polarization of basal bodies in ciliated epithelial cells. *Nat Genet*. 2008; 40:871–9. [PubMed: 18552847]
70. Lee CJ, E.K. K. Gray RS, Park TJ, Wallingford JB. Whole-Mount Fluorescence Immunocytochemistry on *Xenopus* Embryos. *Cold Spring Harbor Protocols*. 2008
71. Sive HL, Grainger RM, Harland RM. *Early Development of Xenopus laevis: A Laboratory Manual*. 2000
72. Soding J. Protein homology detection by HMM-HMM comparison. *Bioinformatics*. 2005; 21:951–60. [PubMed: 15531603]
73. Lobley A, Sadowski MI, Jones DT. pGenTHREADER and pDomTHREADER: new methods for improved protein fold recognition and superfamily discrimination. *Bioinformatics*. 2009; 25:1761–7. [PubMed: 19429599]
74. Hasegawa H, Holm L. Advances and pitfalls of protein structural alignment. *Curr Opin Struct Biol*. 2009; 19:341–8. [PubMed: 19481444]

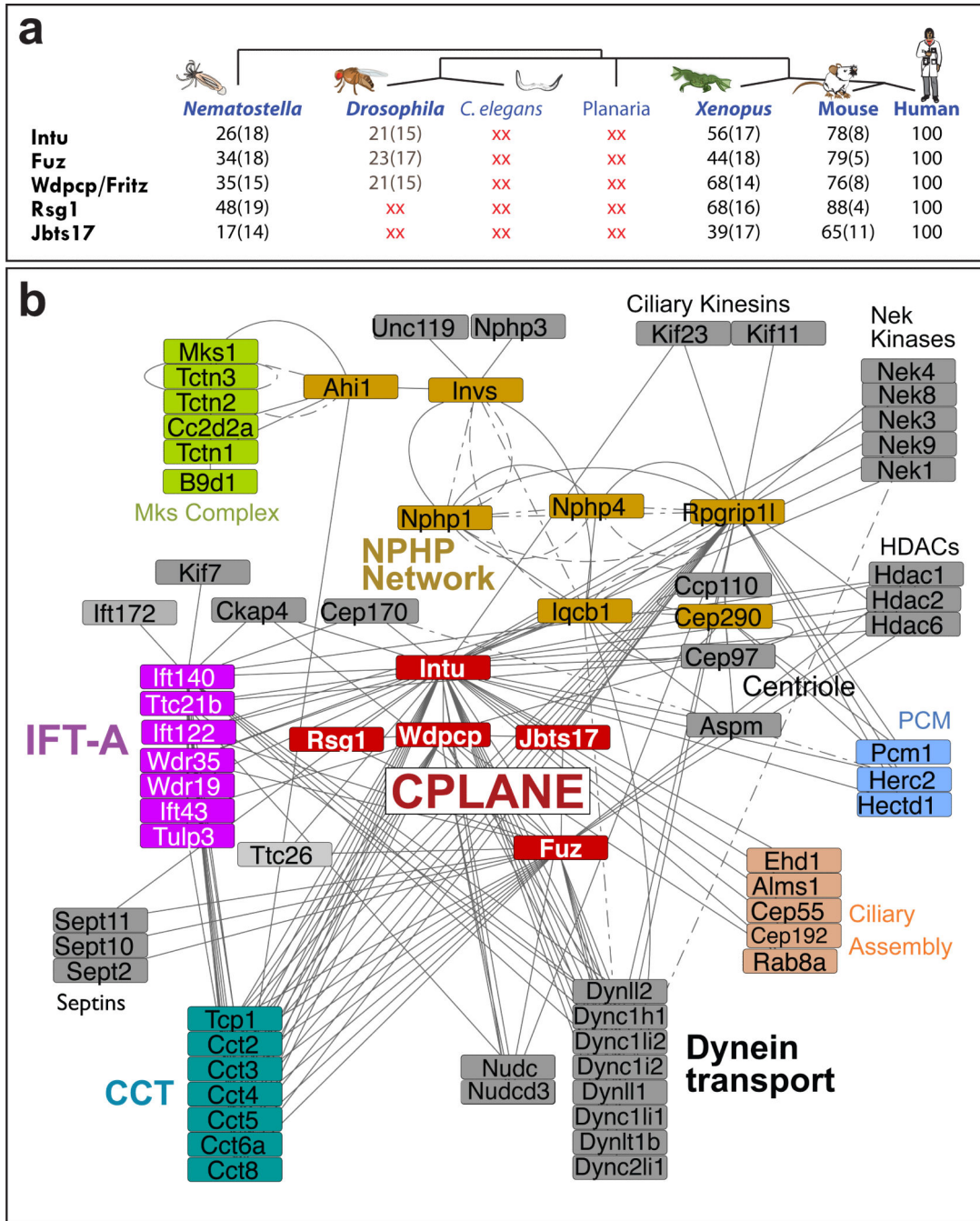


Figure 1. The CPLANE interactome

(a) CPLANE proteins are deeply conserved in evolution; numbers indicate percent identity (+additional percent similarity). “XX” indicates that reciprocal BLAST identified no clear orthologue. (b) The extended CPLANE protein network. Tandem affinity purification of Intu, Fuz, Wdpcp, IFT-A¹⁵, and the published NPHP network⁴ were assembled, thresholded for most likely network members, and over 2200 nodes arranged in Cytoscape, with 78 nodes presented here. The raw peptide data for this network will be deposited in the appropriate databases upon acceptance of the manuscript.

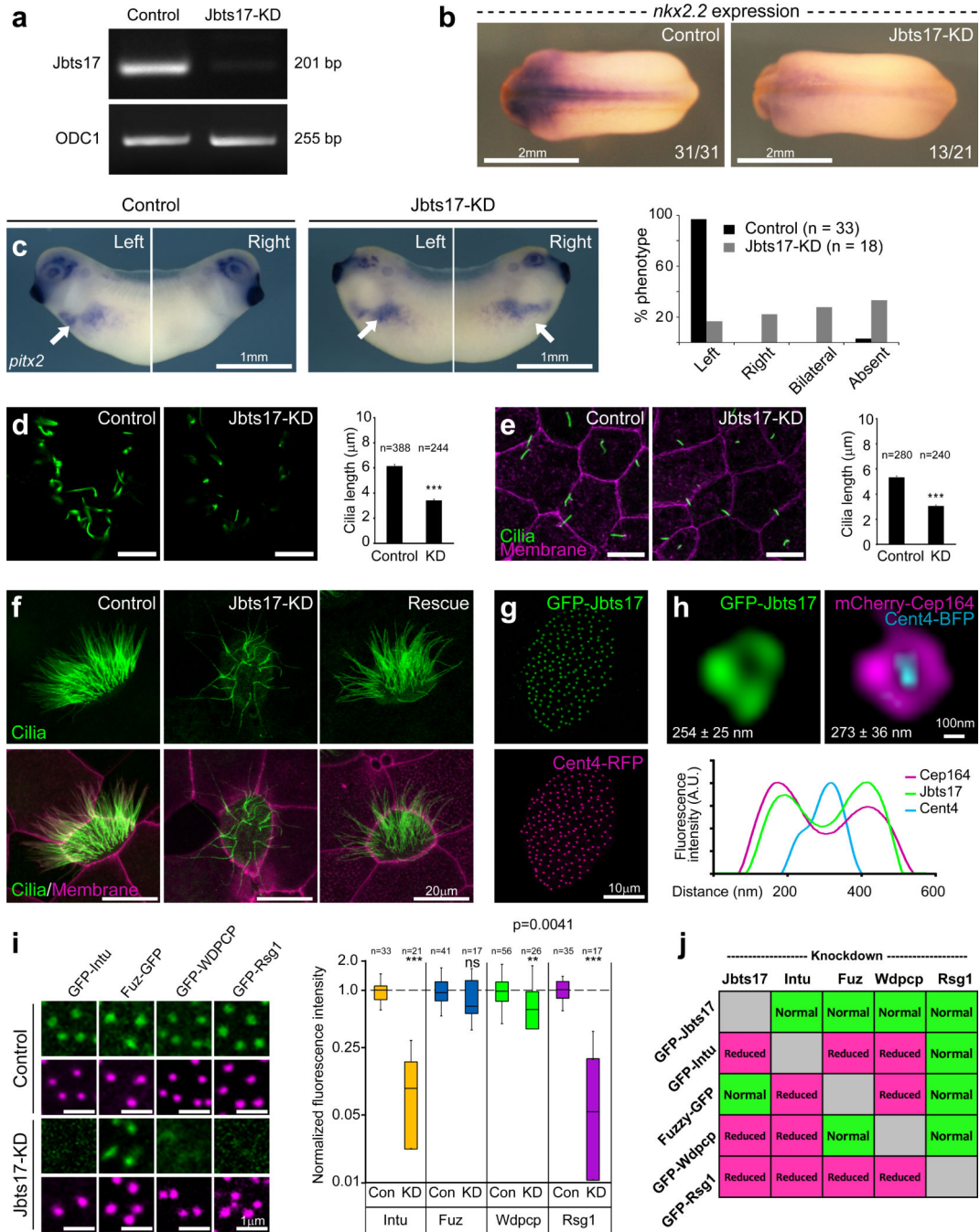


Figure 2. Jbts17 localizes to the base of cilia and is required for ciliogenesis and cilia-mediated patterning

(a) RT-PCR demonstrates disrupted *Jbts17* splicing after MO injection. ODC1 = loading control. (b) *In situ* hybridization of SHH direct target, *nkx2.2* in *Jbts17*-knockdown (st. 22). (c) *Pitx2* expression at st. 26. Arrows indicate signal in left lateral plate mesoderm (LPM); graph indicates *pitx2* expressing embryos. (d) Acetylated α -tubulin immunostaining in the ventral neural tube (st. 22)(Scale bars, 10 μm). (e) Nodal cilia length is reduced; cilia numbers are unchanged. (Scale bars, 10 μm). Graphs in D and E e a c h show pooled data from two independent experiments c i l i a length (mean +/- SEM; ***p < 0.001). (f) Multi-

ciliated cells in control, Jbts17-knockdown (Jbts17-KD), and rescue with untargeted Jbts17 mRNA. Cilia and cell membrane visualized by GFP-CFAP20 (green) and membrane-RFP (magenta). Scale bars, 10 μm . (g) GFP-tagged Jbts17 localizes near basal bodies (visualized by co-expressed centrin4-RFP) in an MCC (scale bar, 10 μm). (h) Super-resolution image of GFP-Jbts17 and mCherry-Cep164 at a single basal body; both form rings of $\sim 260\text{nm}$ around the basal body, visualized by centrin4-BFP. Diameters shown as mean \pm SD in each panel. The lower graph shows fluorescence intensities for GFP-Jbts17, mCherry-Cep164, and centrin4-BFP (Scale bar, 100 nm). (i) GFP-tagged CPLANE proteins (green) and basal bodies visualized by centrin4-RFP (magenta) in control and Jbts17 knockdown multi-ciliated cells; box plots of CPLANE intensities at basal bodies; boxes extend from 25th-75th percentiles, with a line at the median; whiskers indicate max and min. (j) Table summarizes the localization of CPLANE proteins at basal bodies for each knockdown (see Supplementary Fig. 2c-f).

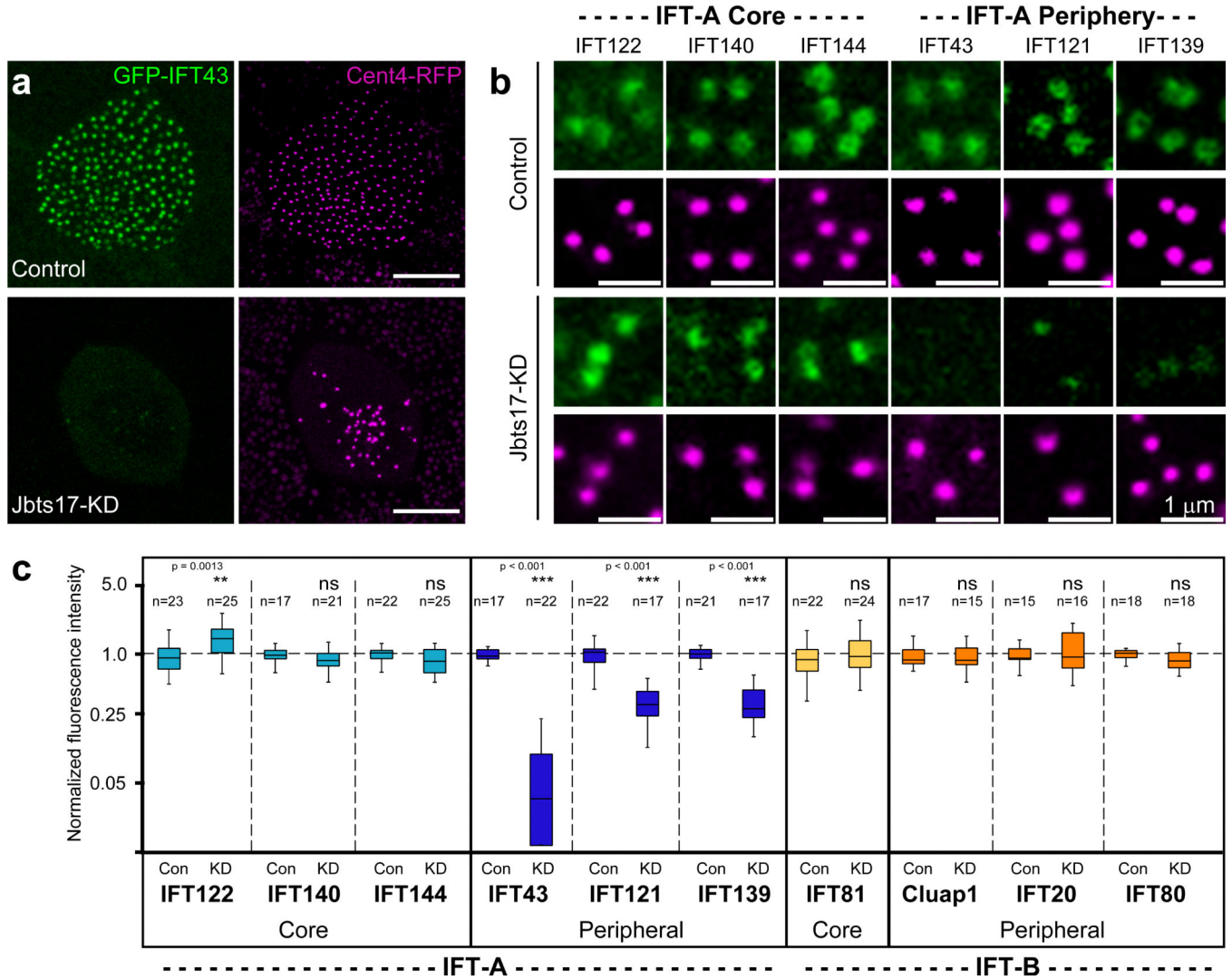


Figure 3. Jbts17 is necessary for recruitment of peripheral IFT-A proteins to basal bodies
 (a) Ift43 localization at basal bodies in *Xenopus* MCCs as marked by centrin4-RFP is lost in MCCs after Jbts17 knockdown. (b) Peripheral IFT-A components are not recruited to centrin4-RFP labeled basal bodies after Jbts17 knockdown. (c) Quantification of IFT protein localization to basal bodies from two independent experiments. Graphs show fluorescence intensity of GFP fusions to indicated IFT proteins normalized against that of centrin4-RFP (see methods). Peripheral IFT-A proteins are specifically lost after Jbts17 knockdown.

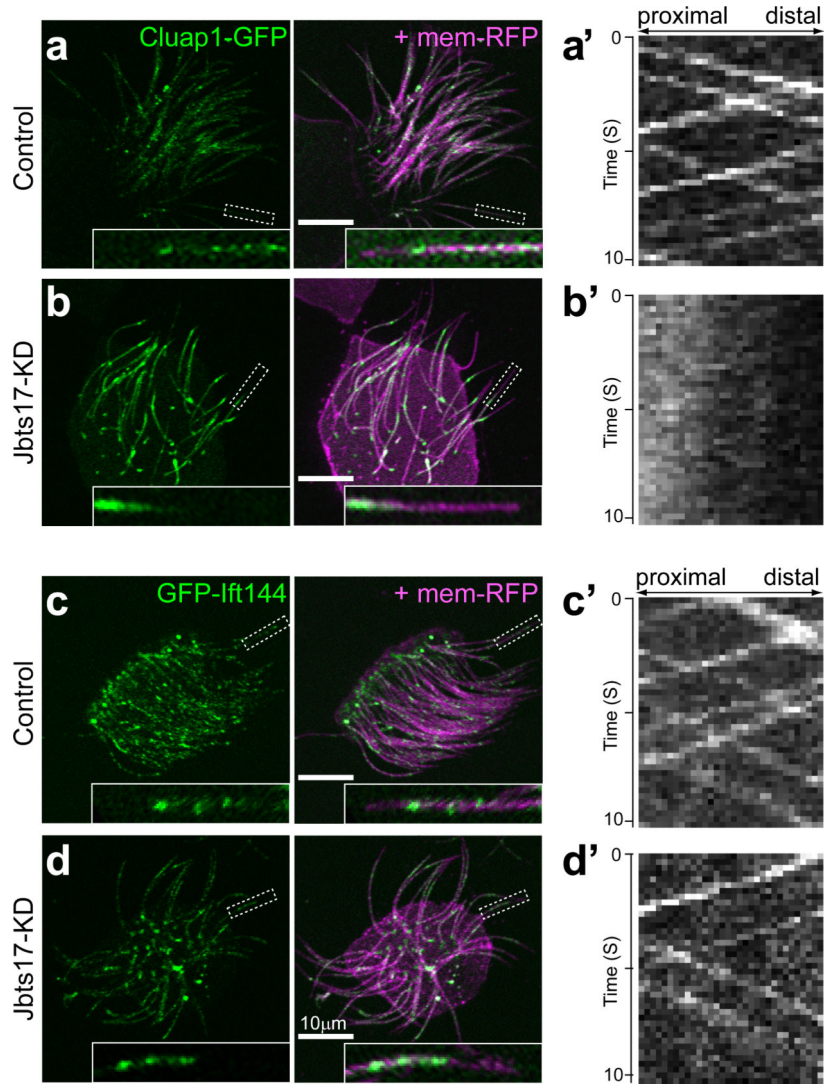


Figure 4. Jbts17 is required for bi-directional axonemal transport of IFT-B particles, but not the core IFT-A

Still images from high-speed time-lapse movies of IFT using GFP fusion to IFT proteins (green) and membrane-RFP (magenta). Cluap1-GFP in control embryo (a) and Jbts17 morphant (b). GFP-IFT144 in control (c) and Jbts17 morphant (d). Insets show high magnification views of localization of IFT particles in a single axoneme in the boxed regions. Scale bars = 10 μm. Associated kymograph representing movements of IFT particles are shown in panels a'-d'.

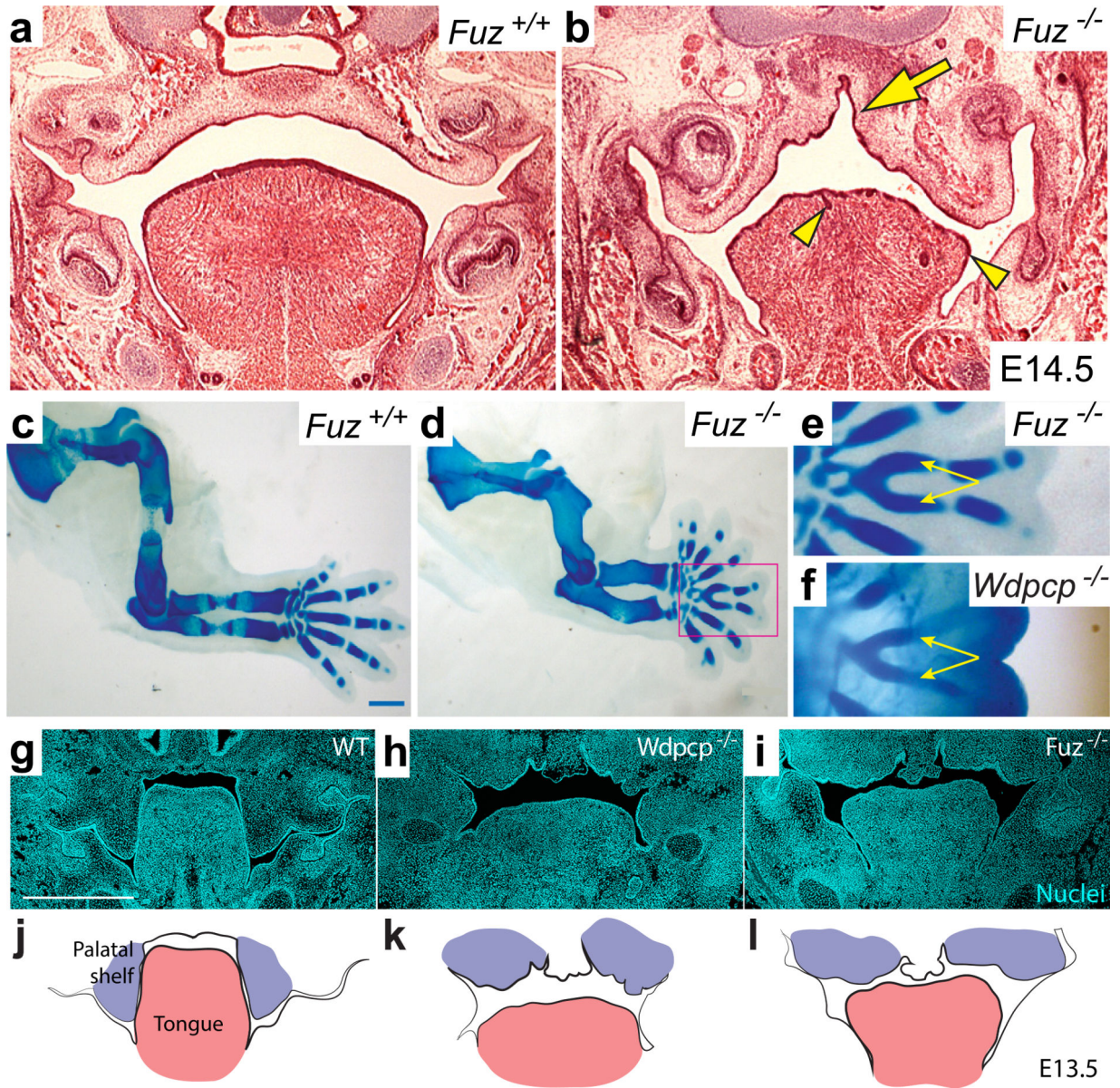
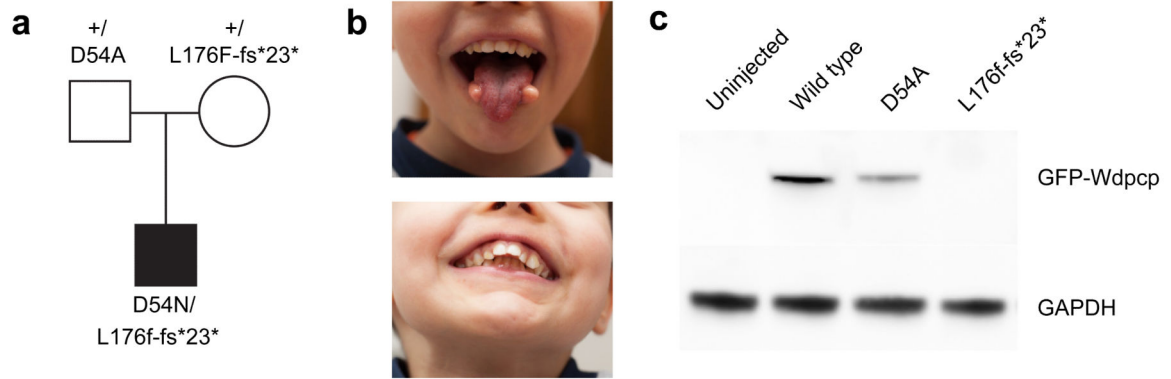
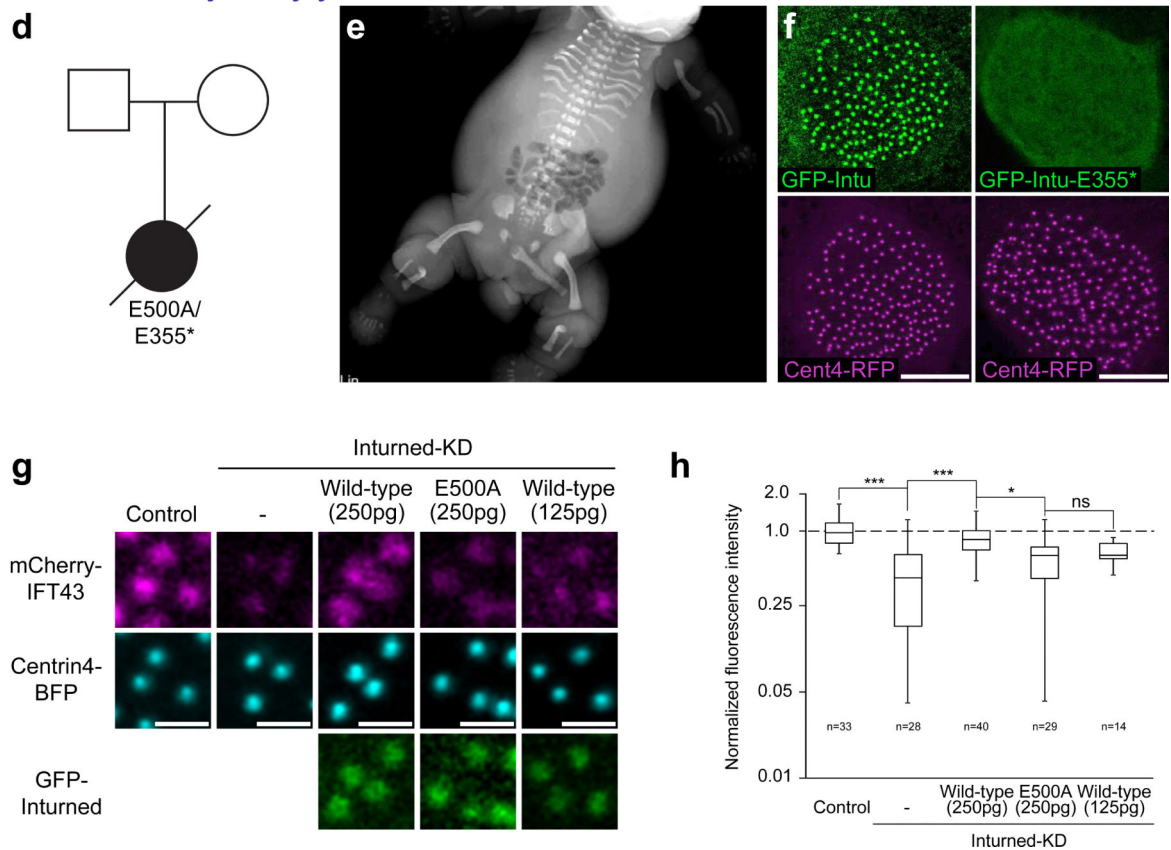


Figure 5. CPLANE mutant mice display diagnostic features of Oral-Facial-Digital Syndrome Type 6

(a and b) Frontal sections at E14.5 reveal that *Fuz* mutant mice display high arched palate (arrow) and lobulation of the tongue (arrowheads). (c and d) *Fuz* mutant mice display develop polydactyly with Y-shaped metacarpals. (e) *Wdpcp* mutant mice display develop polydactyly with Y-shaped metacarpals. (f, g, h) Frontal sections of E13.5 Wildtype, *Wdpcp* and *Fuz* mutant embryos. DAPI labels nuclei (cyan). (f', g', h') Illustrations highlighting the corresponding palatal condensations (purple) and tongue (pink) in F-H. Mutant palatal condensations form more medially than do controls and fail to extend into the mouth (See Tabler et al., 2013).

Oral-Facial-Digital - *WDPCP*Short Rib Poydactyly - *INTU***Figure 6. CPLANE mutations in human ciliopathies**

(a) Pedigree showing *WDPCP* mutations in an OFD patient. (b) The patient displays tongue hamartomas and dental anomalies. (c) When expressed in *Xenopus* embryos, the D54A allele of human *WDPCP* produces less protein compared to wild-type; the L176F-fs26* allele produces no protein. (d) Pedigree showing *INTU* mutations in an SRPS phenotype. (e) X-ray of the patient. (f) The E355* allele of *INTU* disrupts basal body localization. (g and h) Wild-type *Intu* rescues *Ift43* localization to basal bodies after *Intu* knockdown; the E500A allele of *Intu* does not. Data shown are pooled from three independent experiments.

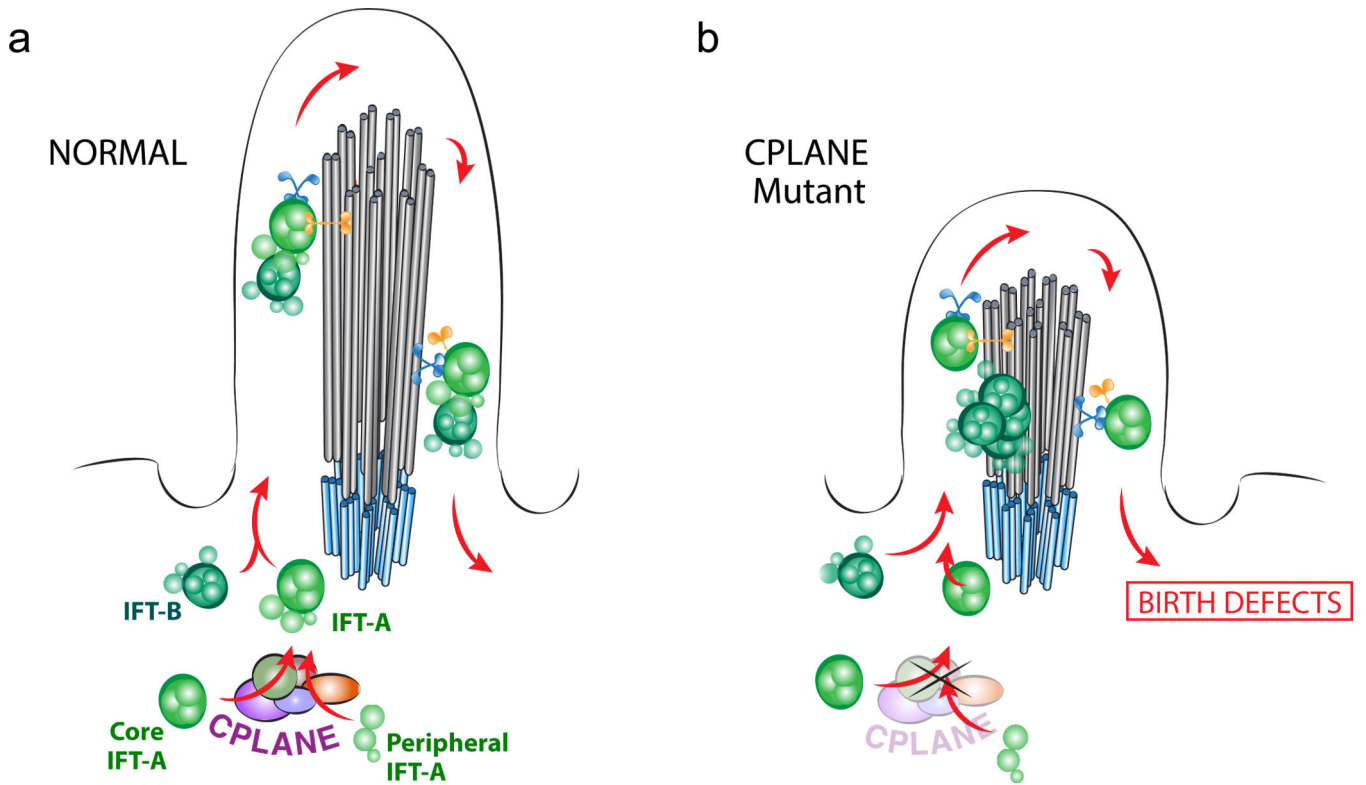


Figure 7. Models for CPLANE function and structure

(a) Schematic of normal IFT. Peripheral proteins are assembled onto the IFT-A core in the cytoplasm and injected together with IFT-B for bi-direction transport in axonemes. (b) In the absence of CPLANE, IFT-A core particles lacking peripheral proteins are injected into axonemes and traffic normally; IFT-B enters axonemes but fails to move in a retrograde direction and accumulates.